Plant Communications
Research Article

CellPress
Partner Journal

Two NPF transporters mediate iron long-distance transport and homeostasis in *Arabidopsis*

Si-Ying Chen[1,2], Tian-Yu Gu[1,3], Zi-Ai Qi[1,2], Jing Yan[1,4], Zi-Jun Fang[1], Yu-Ting Lu[1,2], Hui Li[1] and Ji-Ming Gong[1,2,3,*]

[1]National Key Laboratory of Plant Molecular Genetics, CAS Center for Excellence in Molecular Plant Sciences, Shanghai Institute of Plant Physiology and Ecology, Chinese Academy of Sciences, Shanghai 200032, China

[2]University of the Chinese Academy of Sciences, Beijing 100049, China

[3]School of Life Science and Technology, ShanghaiTech University, Shanghai 201210, China

[4]State Key Laboratory of Crop Stress Adaptation and Improvement, School of Life Sciences, Henan University, Kaifeng 475004, China

***Correspondence: Ji-Ming Gong (jmgong@cemps.ac.cn)**

https://doi.org/10.1016/j.xplc.2021.100244

ABSTRACT

Iron (Fe) transport and reallocation are essential to Fe homeostasis in plants, but it is unclear how Fe homeostasis is regulated, especially under stress. Here we report that NPF5.9 and its close homolog NPF5.8 redundantly regulate Fe transport and reallocation in *Arabidopsis*. *NPF5.9* is highly upregulated in response to Fe deficiency. NPF5.9 expresses preferentially in vasculature tissues and localizes to the *trans*-Golgi network, and NPF5.8 showed a similar expression pattern. Long-distance Fe transport and allocation into aerial parts was significantly increased in *NPF5.9*-overexpressing lines. In the double mutant *npf5.8 npf5.9*, Fe loading in aerial parts and plant growth were decreased, which were partially rescued by Fe supplementation. Further analysis showed that expression of *PYE*, the negative regulator for Fe homeostasis, and its downstream target *NAS4* were significantly altered in the double mutant. NPF5.9 and NPF5.8 were shown to also mediate nitrate uptake and transport, although nitrate and Fe application did not reciprocally affect each other. Our findings uncovered the novel function of NPF5.9 and NPF5.8 in long-distance Fe transport and homeostasis, and further indicated that they possibly mediate nitrate transport and Fe homeostasis independently in *Arabidopsis*.

Key words: NPF transporter, iron homeostasis, nitrate transport and allocation, *trans*-Golgi network

Chen S.-Y., Gu T.-Y., Qi Z.-A., Yan J., Fang Z.-J., Lu Y.-T., Li H., and Gong J.-M. (2021). Two NPF transporters mediate iron long-distance transport and homeostasis in *Arabidopsis*. Plant Comm. **2**, 100244.

INTRODUCTION

Iron (Fe) is an essential microelement for plant growth and development. It is involved in photosynthesis, nitrogen fixation, and other important physiological metabolic processes (Riaz and Guerinot, 2021). Although Fe is abundant in soil, it mainly presents as insoluble Fe^{3+}, which is difficult for plants to acquire, especially in alkaline soil. Higher plants have evolved two strategies to acquire Fe from soil. Nongraminaceous plants adopt the reduction-based mechanism, referred to as strategy I, in which H^+-ATPase secretes protons into the rhizosphere to acidify the soil, thus improving the solubility of Fe^{3+}. It is estimated that Fe solubility increases up to 1000-fold for each unit decrease in pH (Santi and Schmidt, 2009). Fe^{3+} is reduced to more bioavailable Fe^{2+} by the reductase FERRIC CHELATE REDUCTASE (FRO2) and then absorbed into roots by the Fe^{2+} transporter IRT1. Fe deficiency also induces the secretion of phenolics such as coumarin to increase Fe solubility (Siso-Terraza et al., 2016). Fe^{3+} could also be reduced to Fe^{2+} by plasma membrane-localized FRO2 (Connolly et al., 2003) and then translocated into root epidermal cells via the high-affinity Fe^{2+} transporter IRON-REGULATED TRANSPORTER1 (IRT1) (Vert et al., 2002). Graminaceous plants employ strategy II, in which mugineic acids released to the rhizosphere by the deoxymugineic acid efflux transporter TOM1 directly chelate Fe^{3+} to increase Fe solubility (Nozoye et al., 2011), and YELLOW STRIPE-LIKE (YSL) protein is responsible for transport of the Fe(III)–mugineic acid complex (Inoue et al., 2009).

It was considered that Fe was translocated only in chelation form, such as with citrate and nicotianamine (NA) (Curie et al., 2009). FERRIC REDUCTASE DEFECTIVE 3 (FRD3) is responsible for transporting the Fe^{3+}–citrate complex to the

Published by the Plant Communications Shanghai Editorial Office in association with Cell Press, an imprint of Elsevier Inc., on behalf of CSPB and CEMPS, CAS.

xylem in *Arabidopsis thaliana* (Green and Rogers, 2004; Roschzttardtz et al., 2011). OLIGOPEPTIDE TRANSPORTER 3 (OPT3) facilitates Fe recirculation from the xylem to the phloem and regulates shoot-to-root Fe signaling (Mendoza-Cozatl et al., 2014; Zhai et al., 2014). AtYSL2 is responsible for the movement of Fe through the vascular system (DiDonato et al., 2004), AtYSL1 and AtYSL3 are responsible for Fe redistribution in senescent leaves (Waters et al., 2006; Chu et al., 2010), and AtYSL4 and AtYSL6 are located to internal cellular membranes and affect the subcellular transfer of Fe or Fe–NA (Conte et al., 2013; Divol et al., 2013). ZIF1, a homolog of TOM1 in *Arabidopsis*, is located in the vacuolar membrane and speculated to transport NA from cytoplasm to vacuoles, suggesting that NA is involved in the subcellular distribution and interorgan distribution of Fe. Interference in NA transport may have profound effects on Fe use efficiency (Haydon and Cobbett, 2007; Haydon et al., 2012).

The uptake and transport of Fe are also widely affected by other mineral elements. Nitrate has been found to induce Fe-deficiency chlorosis (Smolders et al., 1997). When Fe supply is not adequate, nitrate inhibits the Fe^{3+}–chelate reductase activity in roots but does not affect the uptake capacity for Fe^{2+} (Nikolic et al., 2007). NO_3^- accumulation also increases rhizosphere pH, resulting in chlorotic symptoms (Zhao and Ling, 2007), as roots exude OH^- and HCO_3^- ions during NO_3^- uptake (Nikolic and Romheld, 2003), or alkalinizes the rhizosphere through the H_2O_2-dependent routes of root oxidation ability and phenylpropanoid metabolism (Chen et al., 2018), thus decreasing Fe acquisition. Nitrate reductase can reduce Fe^{3+}–citrate and promote Fe^{2+} translocation and assimilation in plants under conditions of pH 5.5–6.0, which is independent of the process of nitrate reduction in the cytoplasm (Smarrelli and Castignetti, 1988). Further studies demonstrated that NO reduced from NO_3^- by nitrate reductase can enhance the expression of Fe acquisition genes to mediate metal acquisition (Zhai et al., 2016). 2′-Deoxymugineic acid promotes growth of rice by orchestrating Fe and nitrate uptake processes under high pH conditions (Araki et al., 2015). Moreover, it has been reported that the nitrate sensor NRT1.1 may regulate the acquisition of Cd and Fe (Munos et al., 2004; Mao et al., 2014), and the mutation of NRT1.1 enhanced tolerance to Fe deficiency, possibly because less NO_3^- accumulation decreased the FIT (Fe-deficiency-induced transcription factor 1)-dependent Fe acquisition through a feedback mechanism (Liu et al., 2015).

The current research identified and functionally characterized the *NPF5.9*/At3g01350 gene (Leran et al., 2014), which is strongly responsive to Fe starvation. Our study revealed that NPF5.9 preferentially expresses in vascular tissues and localizes to the *trans*-Golgi network. *NPF5.9* overexpression led to leaf chlorosis and enhanced Fe translocation from roots to shoots. *In vitro* assay detected Fe^{2+} and Fe–NA transport activity for NPF5.9 in yeast. A significant phenotype was not observed in the single mutant *npf5.9* or *npf5.8*, but the double mutant *npf5.8 npf5.9* showed apparent alteration in Fe accumulation as well as plant growth and development that can be partially rescued by Fe application. Interestingly, both transporters also mediate nitrate transport, but those Fe-related phenotypes are independent of nitrate availability.

RESULTS

NPF5.9 is highly upregulated under Fe starvation

The interaction between nitrogen and iron nutrition is an interesting topic, but the mechanism is not well understood. To investigate the cross talk, we identified an NPF (NRT1/PTR family) gene, *NPF5.9*, which was strongly induced by iron deficiency through microarray data available in Genevestigator (https://genevestigator.com). Further experimental evidence showed that, compared with the control, *NPF5.9* expression was elevated by around 10 times in both roots and shoots treated with Fe starvation for 3 days (Figure 1A). Tissue level determination of *NPF5.9* expression showed that it is generally low in all the tissues examined, but relatively high expression was observed in roots and flowers of 4-week-old plants (Figure 1B). Similarly, the β-glucuronidase (GUS) activity of *NPF5.9*pro:GUS transgenic plants was obviously enhanced under −Fe conditions (Figure 1C). The spatiotemporal expression analysis indicated that *NPF5.9* expression was detected mainly in the vasculature at seedling stage (Figure 1D). Cross sections of roots further indicated that *NPF5.9* was expressed specifically in pericycle cells (Figure 1E). At the mature stage, *NPF5.9* expression was detected in vascular tissues of leaves (Figure 1F). High-level expression was also detected in flowers, specifically in the upper part of the sepals (Figure 1G) and all over the anthers (Figure 1H), consistent with the qRT-PCR results (Figure 1B).

NPF5.9 showed colocalization with TGN marker SYP61

To investigate the distribution of NPF5.9, we first determined the subcellular localization of an NPF5.9-GFP fusion protein in transgenic lines harboring 35S:NPF5.9-GFP, and the fluorescence of NPF5.9-GFP showed punctate distribution in the cytoplasm (Figure 2A). Moreover, the dot-like fluorescence was also observed in the vasculature of transgenic plants harboring NPF5.9pro:NPF5.9-GFP (Figure 2B). To further determine in which organelle(s) the punctate distribution of NPF5.9 might localize, we performed transient coexpression of NPF5.9-eYFP with organelle markers in *Arabidopsis* protoplasts. The results indicate that NPF5.9 (*35S::NPF5.9-eYFP*) was colocalized with *AtSYP61* (*35S::AtSYP61-mRFP*), a *trans*-Golgi network (TGN)–localization marker (Figure 2B), suggesting that NPF5.9 is likely localized to the apparatus TGN.

Overexpression of *NPF5.9* enhanced Fe translocation to aerial tissues

To evaluate the functional role of NPF5.9 in Fe starvation, we first analyzed *NPF5.9*-overexpressing lines OE5.9-1 and OE5.9-2 (Supplemental Figure 1A and 1B). *NPF5.9* overexpression caused chlorosis in young leaves (Figure 3A). When grown on $^1/_2\times$ MS plates with regular Fe, the rosette size of the overexpressing lines was bigger than that of the wild type (Figure 3A, top), and higher Fe content in young leaves was observed in the overexpressing lines (Figure 3B). When a high level of Fe was added, leaf chlorosis was aggravated and rosette size was apparently reduced in OE5.9-1 and OE5.9-2 compared with Col-0 (Figure 3A, bottom). Furthermore, Fe overaccumulation was also detected in old leaves of OE5.9-1 and OE5.9-2, indicating that Fe overloading into aerial parts occurred and might have resulted in stress under high Fe supply (Figure 3B). Consistently, Fe contents in OE5.9 plant

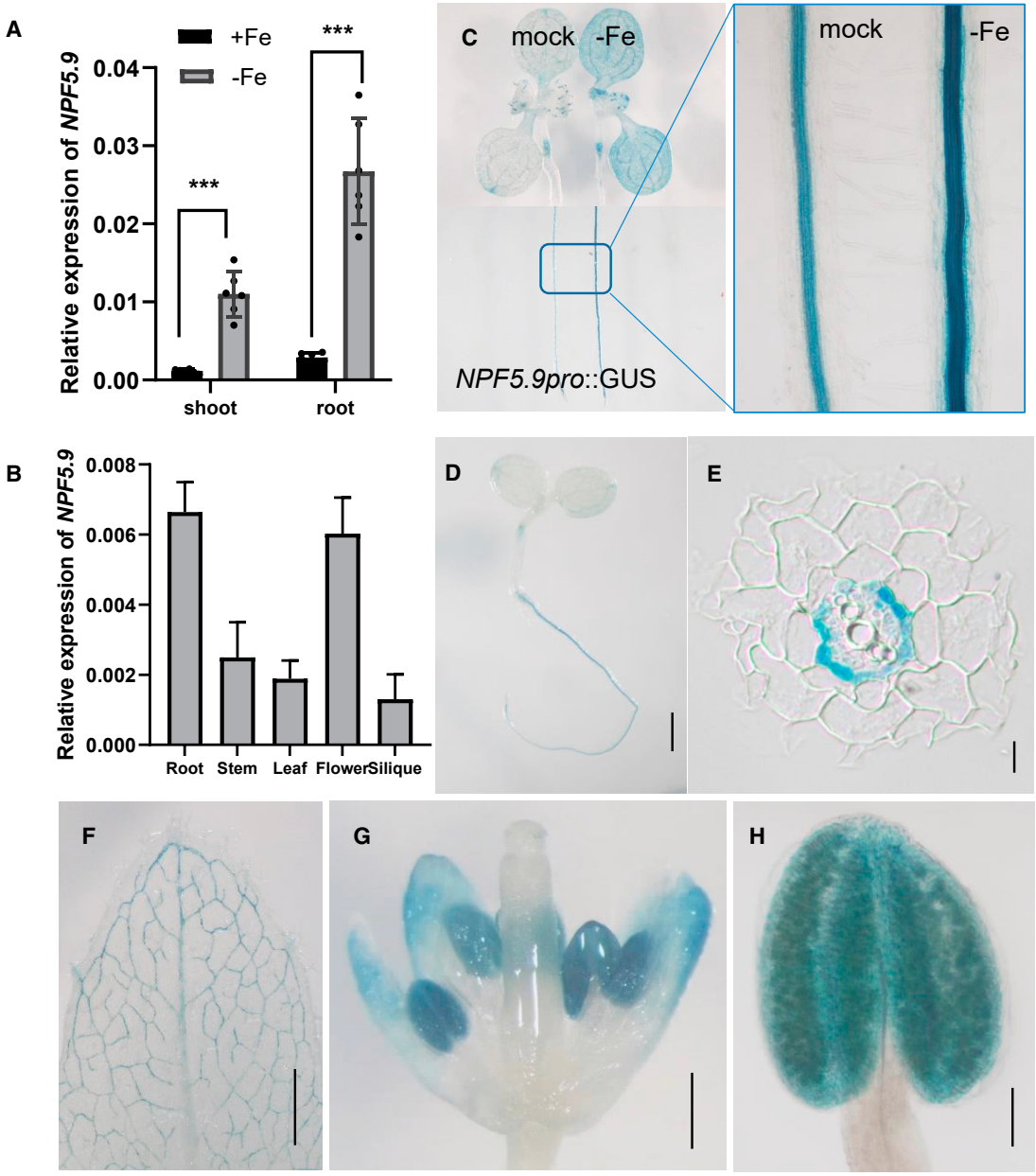

Figure 1. *NPF5.9* expression upon Fe deficiency.

(A) qRT-PCR determination of *NPF5.9* expression in seedling shoots and roots under Fe deficiency. Five-day-old seedings were transferred to medium with (+) or without (−) Fe and grown for 3 days before sampling. Asterisks indicate statistical difference (***$P < 0.001$, Student's *t*-test).

(B) qRT-PCR analysis of *NPF5.9* expression in the root, stem, leaf, flower, and silique. Tissues were harvested from 4-week-old Col-0 plants grown in hydroponic medium. qRT-PCR data were normalized to *Actin2*.

(C) GUS staining of *NPF5.9* pro:GUS transgenic plants in seedlings treated with (mock) or without (−Fe) 2 mM Fe for 24 h.

(D–H) GUS staining in seedlings **(D)**, root pericycle cells **(E)**, leaves **(F)**, flower **(G)**, and anthers **(H)** of transgenic *NPF5.9* pro:GUS plants. Values are the mean ± SD, $n = 6$ in **(A)**, 3 in **(C)**.

Bars, 1 mm in **(D)**, **(F)**, and **(G)**; 0.1 mm in **(H)**; 10 μm in **(E)**.

roots decreased significantly compared with the wild type (Figure 3B). It is interesting that chlorosis still occurred in OE5.9 leaves with Fe overaccumulation, a phenomenon that was also observed in ZIF1-overexpressing plants (Haydon et al., 2012).

When grown to mature age in soil, significant leaf chlorosis was observed in OE5.9-1 and OE5.9-2 compared with Col-0 (Figure 3C). Higher Fe accumulation was steadily detected in rosette leaves, cauline leaves, flowers, and siliques of the overexpressing lines compared with the wild-type control (Figure 3D). Consistently, Fe concentration in xylem sap was also much higher in OE5.9-1 and OE5.9-2 than in the wild-type Col-0 (Figure 3D). *In vitro* assay detected Fe^{2+} and Fe–NA transport activity for NPF5.9 in yeast (Supplemental Figure 2). All these

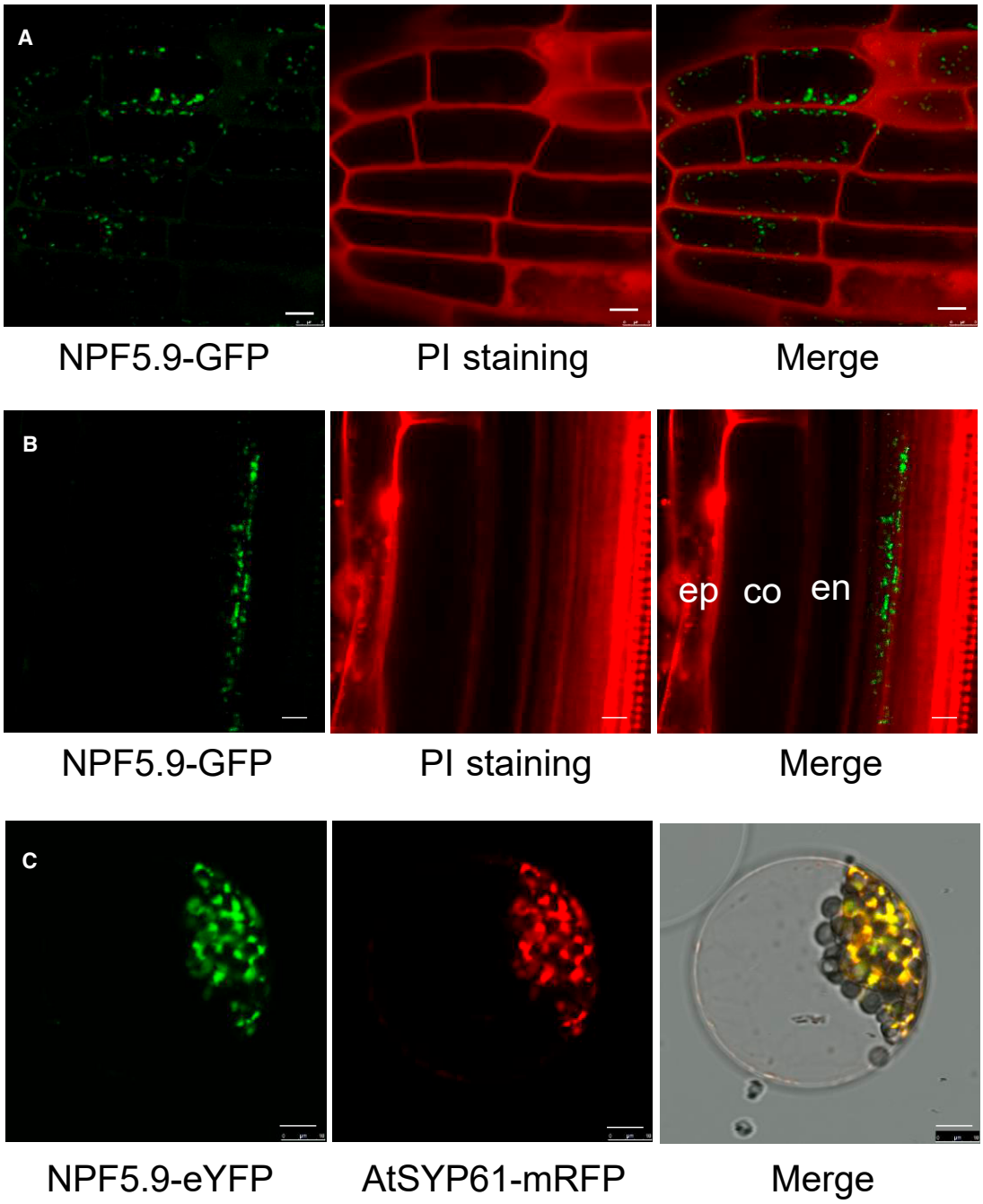

Figure 2. Subcellular localization of NPF5.9 in *trans*-Golgi network.
(A) Fluorescence in root epidermal cells from 4-day-old seedlings of transgenic plants harboring 35S:NPF5.9-GFP.
(B) Fluorescence in root vasculature of 7-day-old transgenic line harboring NPF5.9pro:NPF5.9-GFP. ep, epidermis; co, cortex; en, endodermis. Green or red fluorescence represents GFP or propidium iodide (PI) channels. Bars, 5 μm in **(A** and **B)**.
(C) NPF5.9-eYFP fusion protein colocalization with the *trans*-Golgi network–localized marker AtSYP61-mRFP in *Arabidopsis* protoplasts. Bars, 10 μm.

data suggest that NPF5.9 functions to facilitate Fe bioavailability and long-distance transport to the upper parts in *Arabidopsis*.

Plant growth and Fe allocation were significantly affected in the double mutant *npf5.9 npf5.8*

To further determine NPF5.9's role in Fe starvation response in *Arabidopsis*, two knockout mutants of *NPF5.9* (T-DNA insertion line *npf5.9-T* and CRISPR-Cas9-derived *npf5.9-cr*) were generated and analyzed (Supplemental Figure 1C and 1D). When 5-day-old seedlings were transferred to Fe-deficient plates for 3 days, root elongation of both *npf5.9-cr* and *npf5.9-T* mutants was only slightly slower than that of their corresponding wild-type controls Col-0 and Col-3 (Supplemental Figure 3A), and no significant difference in Fe content was observed between mutant and wild-type plants (Supplemental Figure 3B). Given

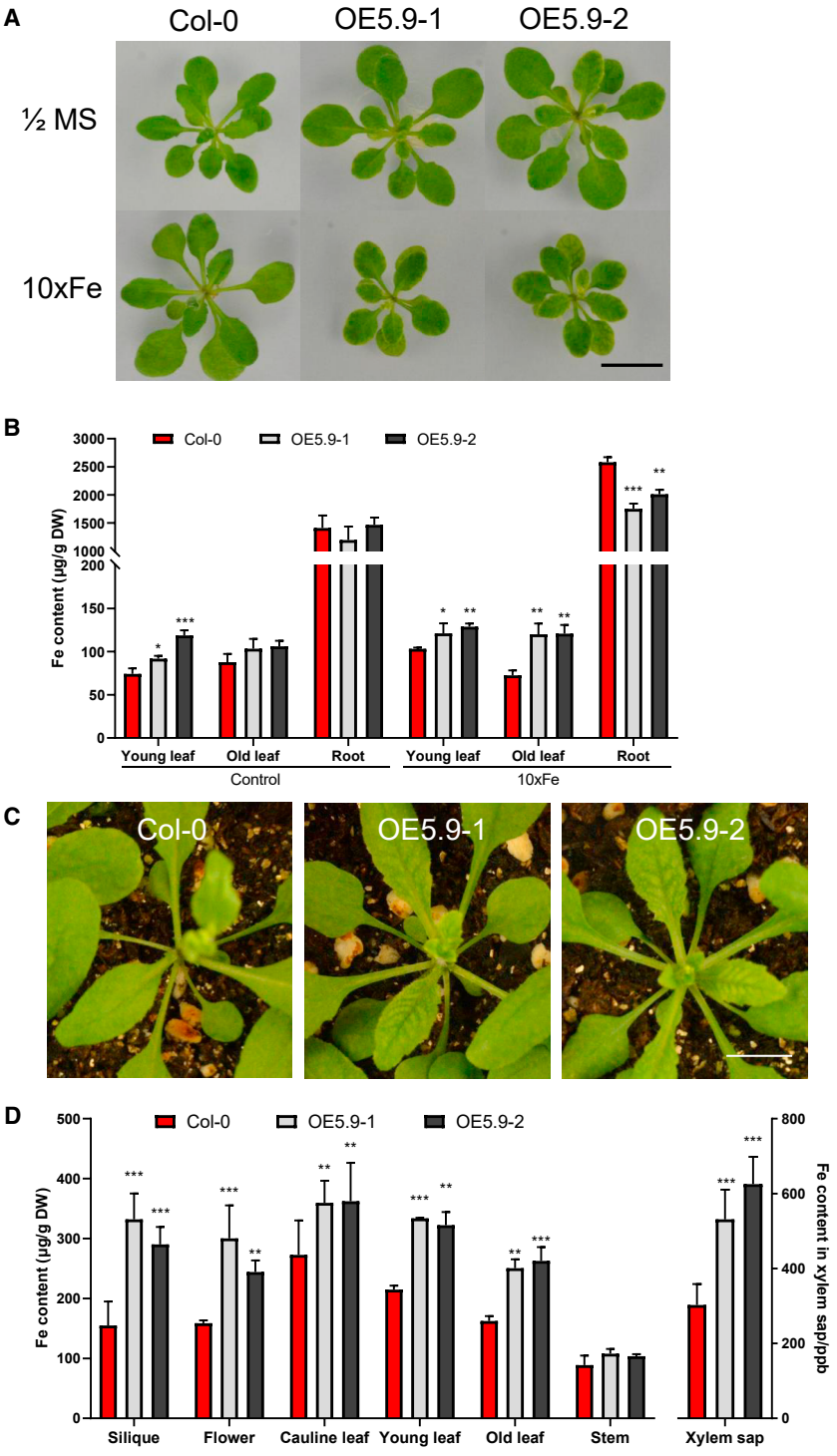

Figure 3. Fe overloading into aerial parts of the *NPF5.9*-overexpressing plants.

(A) The *NPF5.9* overexpression lines OE5.9 and the wild type grown on regular ½ MS medium (½ MS) or with 500 μM Fe-EDTA (10×Fe) for 30 days.

(B) Three-week-old plants grown in hydroponics were treated as indicated for 1 week before sampling for Fe content determination. Control represents condition with regular Fe.

(C) Three-week-old soil-growing overexpression lines exhibit leaf chlorosis compared with wild type. Bar, 1 cm.

(D) Tissues were collected from 5-week-old soil-growing plants, and Fe concentrations were detected in stem, rosette leaf, cauline leaf, flower, silique, and xylem sap by ICP-MS. Values are the mean ± SD, $n = 4$. Asterisks indicate difference at $^{*}P < 0.05$, $^{**}P < 0.01$, and $^{***}P < 0.001$ by Student's *t*-test. Bars, 1 cm in (A and D).

that functional redundancy might occur in NPF5.9 in regulating Fe-related phenotypes, and *NPF5.8* (At5g14940) is the closest homolog to *NPF5.9* in the NPF family (Supplemental Figure 4), showing vasculature-specific expression pattern (Supplemental Figure 5A–5F) and similar subcellular localization (Supplemental Figure 5G), we then generated and analyzed *npf5.8-1*, *npf5.8-2*, and *npf5.8-3* mutants using the CRISPR-Cas9 system (Supplemental Figure 1E). Similar results were obtained (Supplemental Figure 3C and 3D), except that a more significant root elongation defect was observed in *npf5.8* than in *npf5.9*. We also measured spatial Fe distribution by using Perls/DAB staining, but still no significant change was observed (Supplemental Figure 3E).

To further test if functional redundancy does occur, we generated the double mutants *dm-1(npf5.8-1 npf5.9-cr)*, *dm-2(npf5.8-3 npf5.9-cr)*, *dm-3(npf5.8-1 npf5.9-T)*, *dm-4(npf5.8-2 npf5.9-T)*, and *dm-5(npf5.8-3 npf5.9-T)* by genetic crossing. All these double mutants showed serious defects in seed germination (Supplemental Figure 6A, left), and enhanced Fe application did not rescue the germination defect (Supplemental Figure 6A, right). Consistent phenotypes were observed in all five independent lines, and representative *dm-3/dm-2* were selected for further analysis. As shown in Supplemental Figure 6B, the overall plant growth of the double mutant was affected even when at seedling age. During the vegetative growth period, *npf5.8 npf5.9* mutants showed leaf chlorosis, and irrigation of Fe restored the green color of leaves (Figure 4A). During the reproductive growth period, both plant growth and silique development were severely affected and partially restored by Fe addition (Figure 4B–4D). Further analysis showed that Fe content in xylem sap was decreased in the double mutant (Figure 5A), although Fe accumulation in roots did not increase as we expected (Figure 5B), which might be attributable to the overall lower Fe uptake as indicated by the constitutively high expression of *IRT1* and *FRO2* in the double mutants (Figure 6). Fe content in rosette leaves and flowers of the double-mutant plants was lower than that in the wild-type Col-0 when irrigated with water (Figure 5C). Interestingly, irrigation with Fe restored Fe accumulation in rosette leaves but not in flowers

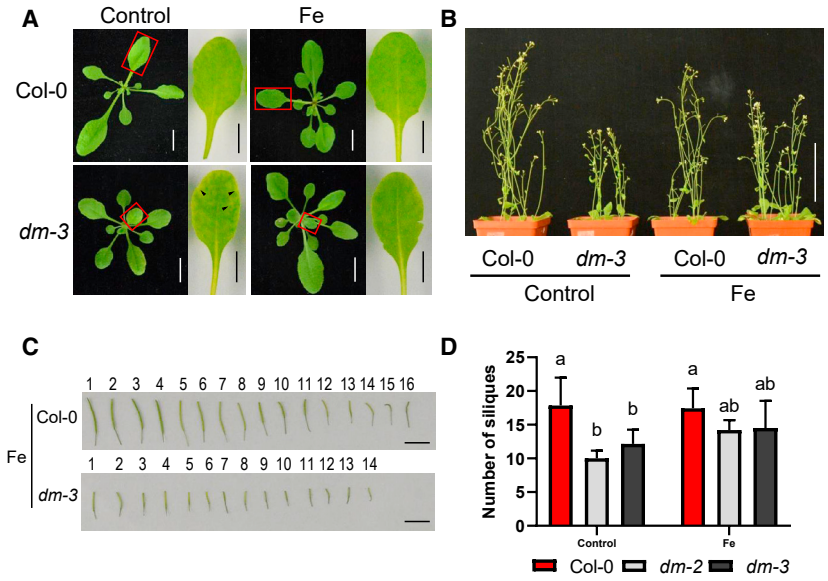

Figure 4. Leaf chlorosis and altered plant growth in the *npf5.8 npf5.9* double mutants.
(A and **B)** Col-0 and *npf5.8 npf5.9* double mutants (*dm-2*, *dm-3*) were grown in soil watered with (Fe) or without (control) 0.5 mM Fe-EDDHA, and leaf chlorosis at 3 weeks of age **(A)** or plant growth at 4 weeks of age **(B)** was imaged. White bar, 1 cm in **(A)** or 10 cm in **(B)**; black bar, 5 mm. In **(A), red boxes on the left outline leaves shown magnified on the right.** Black arrowheads indicate leaf chlorosis.
(C) Representative images of siliques of 4-week-old Col-0 and the *npf5.8 npf5.9* double mutant watered with 0.5 mM Fe-EDDHA. Bar, 1 cm.
(D) Silique numbers of Col-0 and the *npf5.8 npf5.9* double mutants from **(C)**. Values are the mean ± SD, $n = 7$. Different letters show significant differences at $P < 0.05$ by two-way ANOVA.

(Figure 5C). No significant difference was observed between siliques of the mutant and the wild-type plants on irrigation with either water or Fe (Figure 5C). These results, together with those from Figure 3, indicate that NPF5.9 and NPF5.8 function to mediate Fe translocation to leaves, and disruption of this process might essentially affect Fe homeostasis.

Disturbed gene expression in *npf5.8 npf5.9* double mutants

We further determined the expression levels of genes related to either Fe nutrition or nitrate uptake. The results showed that when supplied with adequate Fe, most of the investigated genes showed comparable expression between the wild type and the double mutant (Figure 6), except that *IRT1* and *FRO2*, two important genes involved in Fe uptake, were expressed at significantly higher levels in the double mutant (Figure 6), indicating higher demand for Fe in the mutant. When under Fe starvation conditions, both *IRT1* and *FRO2* were induced to much higher level, but the levels were comparable between the wild type and the mutant. In contrast, *PYE* and *BTS*, the negative regulators of the iron-deficiency response (Long et al., 2010; Hindt et al., 2017; Tissot et al., 2019), were also upregulated in response to Fe starvation, but the induction was significantly lower in the mutant than in the wild-type plants. *NAS4*, which is a downstream component of the PYE, also showed lower expression in the mutant (Figure 6). Interestingly, the gene related to nitrate uptake (*NRT1.1*) also showed significantly lower expression in the mutant when under Fe starvation. These observations indicate that, although NPF5.9 and NPF5.8 function mainly in Fe reutilization, they might also contribute to the feedback regulation deriving from the complicated iron homeostasis.

NPF5.9 and NPF5.8 also mediate nitrate allocation independent of Fe status

As NPF family members are critical players in nitrate uptake and allocation, we then determined if NPF5.9 and NPF5.8 also transport nitrate. Electrophysiological analysis showed that significantly higher inward currents were detected in oocytes injected with *NPF5.9* cRNA compared with those injected with water (Figure 7A). Nitrate uptake assay showed that both NPF5.9 and NPF5.8 mediate regular pH-dependent low-affinity nitrate uptake (Figure 7B). In the double-mutant plants, nitrate concentration decreased in xylem sap while it increased in rosette leaves of the mutant (Figure 7C). These results suggest that NPF5.8 and NPF5.9 do mediate nitrate allocation *in planta*.

To investigate the possible interaction between iron homeostasis and nitrate transport mediated by NPF5.8 and NPF5.9, we then determined if supplementation with nitrate or Fe would reciprocally affect each other. The data showed that in *npf5.8 npf5.9* double-mutant plants, nitrate application did not rescue the Fe-related growth defect (Supplemental Figure 7), and the nitrate accumulation pattern in both leaves and roots was not affected by Fe addition or depletion (Figure 7D and 7E). In the overexpressing lines, leaf chlorosis was not altered despite the nitrate status (Supplemental Figure 8). These results suggest that the nitrate transport function of NPF5.8 and NPF5.9 is probably not involved in its Fe translocation, and NPF5.9-mediated Fe translocation and nitrate uptake are two relatively independent biological processes.

DISCUSSION

Fe transport and reallocation play a pivotal role in plant Fe nutrition. Our study identified a novel NPF transporter gene, *NPF5.9*, which is highly upregulated in response to Fe deficiency. *NPF5.9* is expressed preferentially in vasculature tissues, and Fe long-distance transport and accumulation in aerial parts was significantly increased in *NPF5.9*-overexpressing lines, while in the double mutant *npf5.8 npf5.9*, both Fe content and plant growth were decreased, consistently indicating that both transporters mediate Fe mobility in *Arabidopsis* and represent two novel regulators in Fe homeostasis. We also identified NPF5.9 and NPF5.8 as two nitrate transporters functioning in a low-affinity and pH-dependent manner in oocytes. However, to our surprise, they appeared to mediate Fe allocation and accumulation independent of its nitrate transport function (Figure 7, Supplemental Figures 7 and 8).

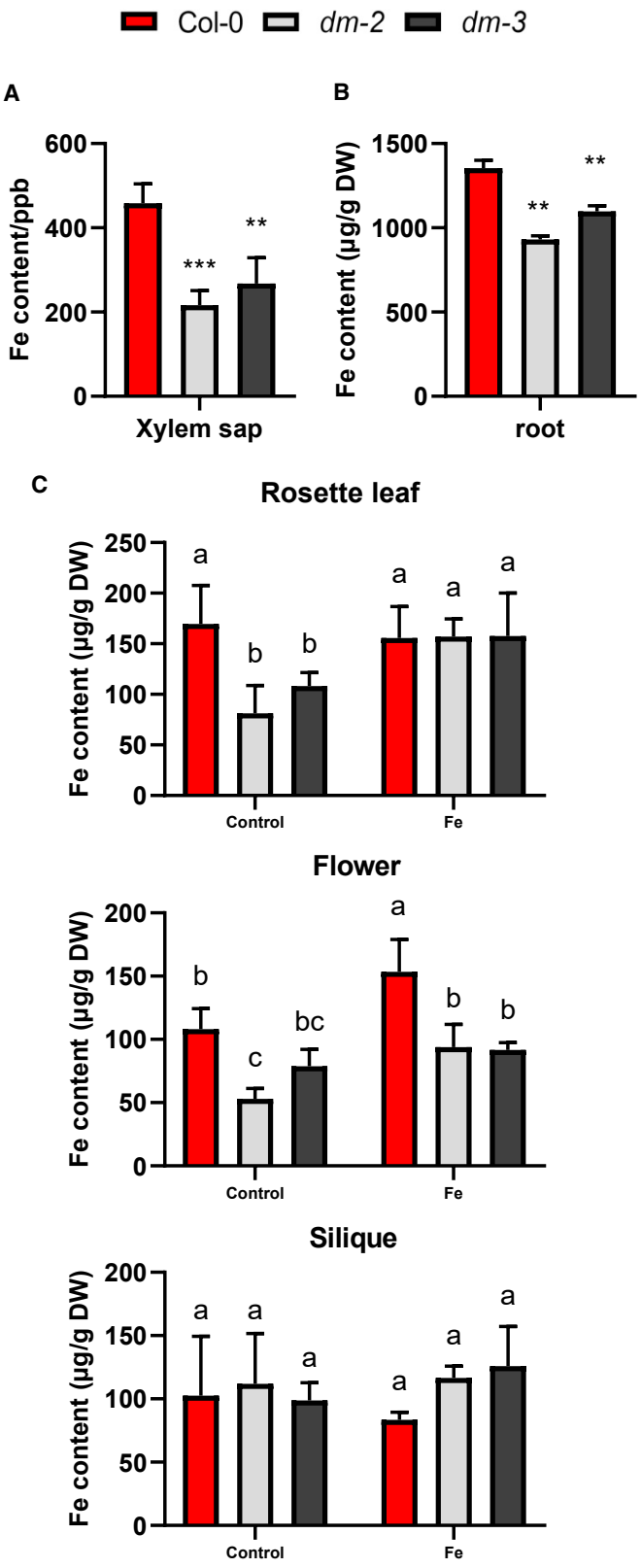

Figure 5. Decreased Fe accumulation in *npf5.8 npf5.9* and recovery of leafy Fe by iron feeding.

(A) Xylem sap was collected from 4-week-old plants grown in soil to measure Fe content.

(B) Fe content in roots of 2-week-old plants grown in hydroponics.

(C) Plants grown in soil were irrigated with water (control) or 0.5 mM Fe-EDDHA (Fe) to 4 weeks of age, and Fe content was analyzed in rosette leaves, flowers, or siliques. Values are the mean ± SD, $n = 4$. Asterisks in **(A** and **B)** indicate difference at $^{**}P < 0.01$ or $^{***}P < 0.001$ compared with Col-0 by Student's *t*-test. Different letters in **(C)** above the bars show significant differences at $P < 0.05$ by two-way ANOVA.

Although the NPF family has not been reported to transport Fe, several studies did find they transport a wide range of substrates in addition to nitrate. *Arabidopsis* NRT1.1 is the first identified nitrate transporter and functions in both dual-affinity nitrate transport and nitrate sensing (Tsay et al., 1993; Liu et al., 1999), and it was later found that NRT1.1 also transports auxin outward to inhibit lateral root growth under low nitrate utilization (Krouk et al., 2010). In addition, OsNRT1.1b was discovered to have both nitrate and selenomethionine transport activity in rice (Zhang et al., 2019). *Arabidopsis* NRT1.5 is responsible for nitrate loading into xylem vessels (Lin et al., 2008), and recent research revealed that it also mediates indole-3-butyric acid uptake into specific cells to ensure proper auxin gradient (Watanabe et al., 2020). More small molecules, such as ABA, GA, 4MTB, JA-Ile, and dipeptides, have also been identified as substrates of the NPF family members (Corratge-Faillie and Lacombe, 2017). From these observations, it is very likely that NPF5.9 and NPF5.8 do have two distinct functions, and they mediate Fe transport and homeostasis via substrates other than nitrate.

Due to the insolubility and toxicity of Fe ion, Fe generally presents and mobilizes in the complex forms of Fe^{2+}–NA and Fe^{3+}–citrate (Ravet et al., 2009), and these complexes are translocated through pericycle cells and loaded into the vasculature (Connorton et al., 2017); thus it is very likely that NPF5.9 and NPF5.8 mediate the transport of one of these complexes. Our current research provided several pieces of evidence that are supportive of this postulation. First, it has been reported that TGN-localized NRAMP2 is responsible for building up the Mn pool in the cytosol to supply Mn for downstream organelles, such as vacuoles, chloroplasts, and mitochondria (Alejandro et al., 2017), while NPF5.9 is located in the endomembrane system TGN (Figure 2C) and is expressed mainly in vasculature tissues. Second, previous studies showed that *nas4x*, in which NA synthase and Fe reallocation were disrupted, displayed leafy chlorosis and Fe accumulation similar to those observed in the NFP5.9-overexpressing plants (Klatte et al., 2009; Figure 3A and 3C, Supplemental Figure 8), and *NAS4* expression upon Fe starvation was significantly decreased in the double mutant (Figure 6). Third, we roughly measured iron uptake in the uptake-defective yeast mutant *fet3fet4*, and the results did indicate essential uptake of the Fe–NA complex and possibly Fe^{2+} (Supplemental Figure 2). From this aspect, we speculate that NPF5.9 might transport Fe–NA, hence making the TGN serve as an intracellular Fe pool for further reallocation within plants.

METHODS

Plant growth conditions and materials

Seeds were surface sterilized and germinated for 5 days on ½ MS with 0.1% MES, 1.5% (for vertical growth) or 0.8% (for horizontal growth) agar (pH 5.8) at 21°C–23°C with 60% relative humidity and a 16-h light/8-h dark photoperiod. The seedlings were then grown on ½ MS with treatment of −Fe (0 μM Fe + 150 μM ferrozine), +Fe (regular Fe), or 10×Fe (500 μM Fe-EDTA), for the indicated times, or combined with

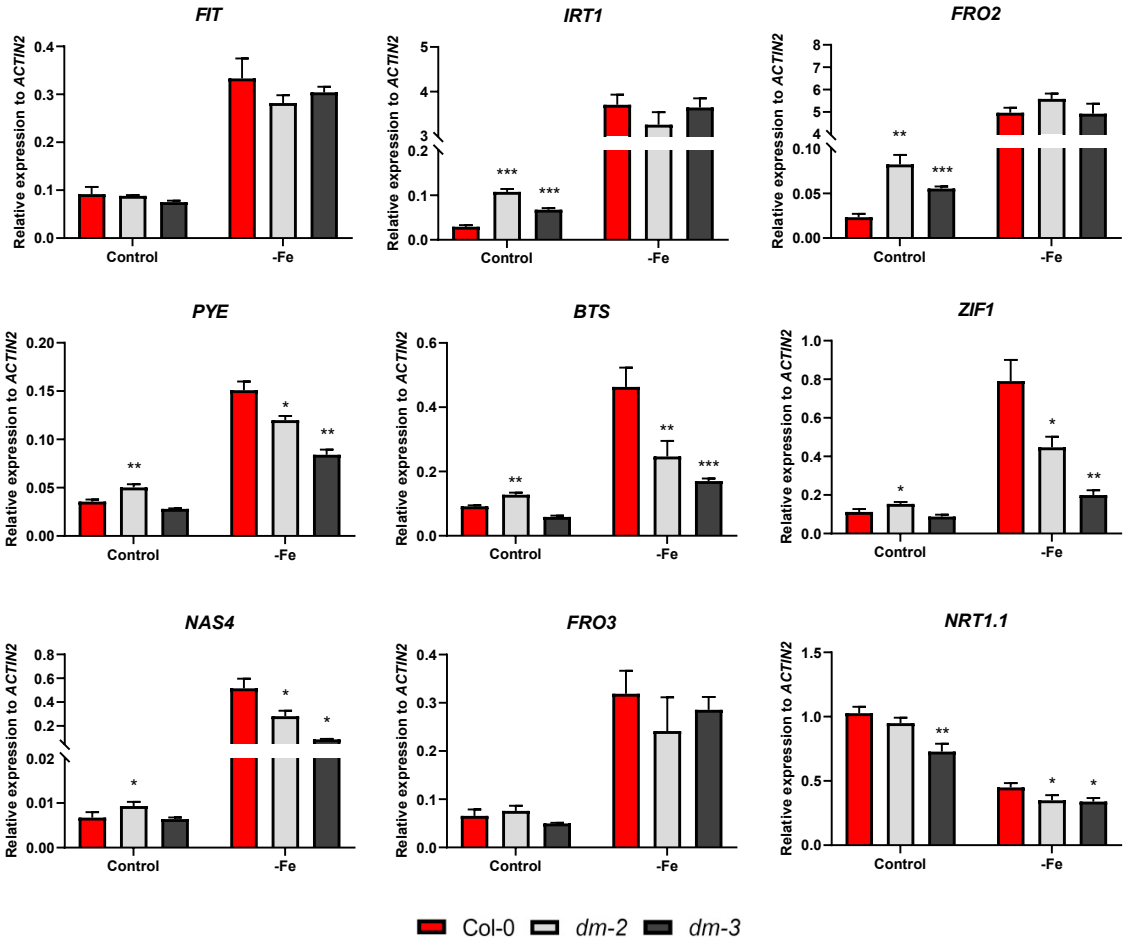

Figure 6. Altered gene expression in *npf5.8 npf5.9* double mutant.
Fourteen-day-old wild type and double mutants were transferred to hydroponic solutions with regular Fe (control) or Fe starvation (−Fe) for 72 h before sampling to extract RNA. Relative expression was determined by real-time RT-PCR for the Fe uptake regulator *FIT* and its downstream genes *IRT1* and *FRO2*; Fe transport and sequestration genes *NAS4*, *FRO3*, and *ZIF1* and their negative regulator *PYE*; the negative regulator *BTS* of the iron-deficiency response; and the nitrate transceptor *NRT1.1*. Values are the mean ± SD, $n = 4$. Asterisks indicate difference at $^{*}P < 0.05$, $^{**}P < 0.01$, or $^{***}P < 0.001$ compared with Col-0 by Student's *t*-test.

treatment of different concentrations of NH_4NO_3 as indicated. Alternatively, seedlings were transferred to hydroponic solution and grown for ~3 weeks as described (Gong et al., 2004) and then further exposed to Fe starvation (−Fe) for 10 days.

The T-DNA insertion mutant *npf5.9-T* in the Col-3 background was purchased from NASC (European *Arabidopsis* Stock Center) and identified by PCR. *npf5.9-cr* and *npf5.8* in the Col-0 background were generated in our lab by the CRISPR-Cas9 system. The double mutant *npf5.8 npf5.9* was generated by crossing *npf5.8-1/-2/-3* and *npf5.9-cr/npf5.9-T* and screening homozygotes by PCR and sequencing. NPF5.9-overexpressing plants were generated by transforming the construct *35S::NPF5.9-GFP/pCAMBIA1301* into Col-0. Putative transformants were selected on $^1/_2$ MS plates containing 0.0025% (w/v) hygromycin B. The primers used here are listed in Supplemental Table 1.

Quantitative real-time PCR

Total RNA was extracted using TRIzol reagent (Invitrogen). cDNAs were synthesized using oligo(dT) primers and PrimeScript RT Enzyme Mix I (TaKaRa). Quantitative PCR was performed with the CFX Connect real-time system (Bio-Rad) using SYBR Premix Ex-Taq HS (TaKaRa) according to the manufacturer's protocol. Primers used in these assays are listed in Supplemental Table 1, and expression data were normalized to *Actin2*.

Functional analysis of NPF5.9 in *Xenopus laevis* oocytes

The coding DNA sequence of *NPF5.9* was introduced into the *pOO2* vector. The *NPF5.9/pOO2* plasmids were linearized using *Mlu*I, and capped mRNA was transcribed *in vitro* using mMESSAGE mMACHINE kits (Ambion). Oocytes were isolated and injected with 50 ng of *NPF5.9* cRNA in 50 nl of water, as described (Tsay et al., 1993). After incubation in the ND96 solution containing 0.005% (w/v) gentamycin for 48 h, nitrate uptake assays using [^{15}N]nitrate were performed using a continuous-flow isotope ratio mass spectrometer coupled with a carbon nitrogen elemental analyzer (Thermo Scientific EA IsoLink IRMS System). *CHL1* cRNA and water-injected oocytes were used as positive and negative controls, respectively. Electrophysiological analysis of injected oocytes was performed as described (He et al., 2017). After incubation for 48 h, oocytes were voltage clamped at −60 mV and perfused with 10 mM nitrate at pH 5.5.

Histochemical localization

A 2793-bp genomic fragment upstream of the *NPF5.9* start codon was amplified using primers listed in Supplemental Table 1. The fragments were verified by sequencing and cloned into the binary vector *GUS/pCAMBIA1300*, which was then transformed into Col-0 by the *Agrobacterium tumefaciens*–mediated floral dip method as described

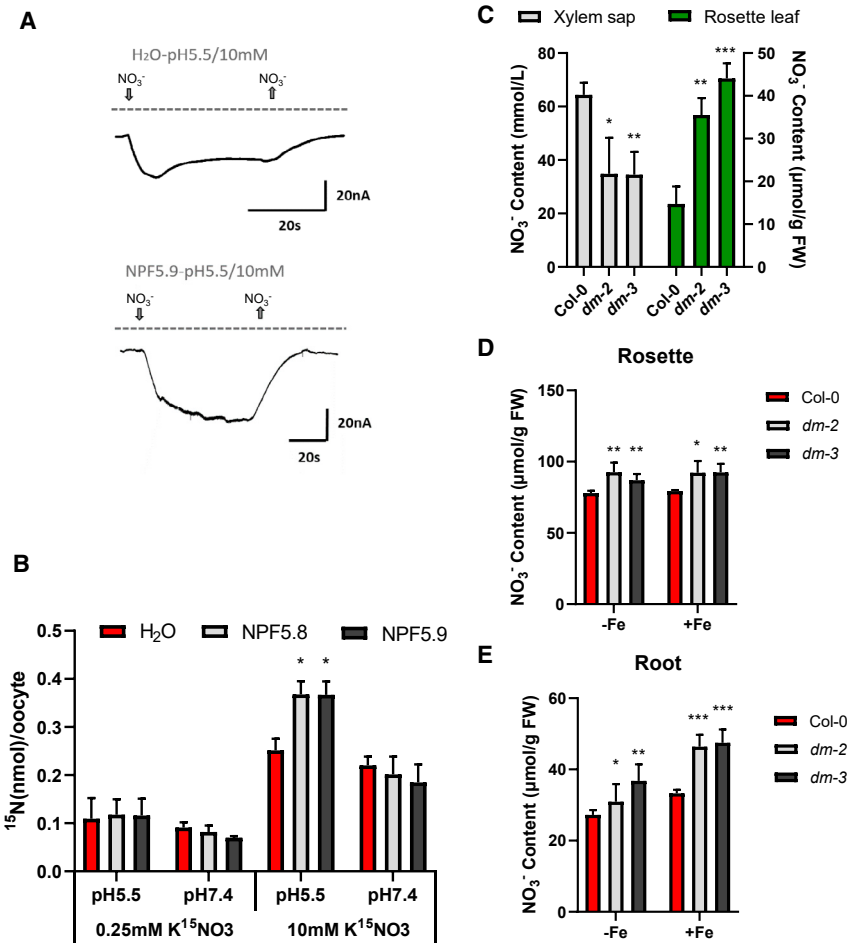

Figure 7. NPF5.9 and NPF5.8 mediate nitrate transport.

(A) Representative inward currents elicited by 10 mM NO_3^- at pH 5.5 and a holding potential of −60 mV were recorded in a single oocyte injected with H_2O (top) or *NPF5.9* cRNA (bottom).

(B) High- or low-affinity nitrate uptake activity of NPF5.8 and NPF5.9. Oocytes injected with H_2O, *NPF5.8* cRNA, or *NPF5.9* cRNA were incubated with 0.25 mM $^{15}NO_3^-$ at pH 5.5/pH 7.4 or 10 mM $^{15}NO_3^-$ at pH 5.5/pH 7.4 for 3 h. Values are means ± SD, $n = 6–8$. Asterisks indicate difference (*$P < 0.05$ Student's *t*-test).

(C) Determination of nitrate in xylem sap and rosette leaves from 4-week-old plants grown in soil.

(D E) Three-week-old plants grown in hydroponics were subjected to Fe starvation for 3 days, and nitrate content in rosette leaves **(D)** and roots **(E)** were analyzed by high-performance liquid chromatography. Values are means ± SD, $n = 4$. Asterisks indicate difference at *$P < 0.05$, **$P < 0.01$, or ***$P < 0.001$ in the double mutants compared with wild-type Col-0 by Student's *t*-test.

(Clough and Bent, 1998). Putative transformants were selected on ½ MS plates containing 0.0025% (w/v) hygromycin B. GUS staining was performed with plants at the indicated age as described (Luo et al., 2018), with minor modification. Samples were vacuum infiltrated for 5 min and then incubated for 3 h in GUS staining buffer containing 50 mM $NaPO_4$ (pH 7.4), 5 mM ferrocyanide, 5 mM ferricyanide, 0.05% Triton X-100, and 1 mM 5-bromo-4-chloro-3-indolyl-β-D-glucuronide. Thin cross sections (8 μm) were generated using a Leica RM 2165 microtome and imaged using the Nikon-SMA800.

Subcellular localization

The coding sequences of *NPF5.9*, *NPF5.8*, and *AtSYP61* were isolated by PCR, and the PCR products were confirmed by sequencing before subcloning into the vector *35S::eYFP/pA7* or *35S::mRFP/pA7*. The resulting constructs *35S::NPF5.9-eYFP/pA7*, *35S::NPF5.8-eYFP/pA7*, and *35S::AtSYP61-mRFP/pA7* were transiently expressed in *Arabidopsis* protoplasts using the polyethylene glycol–mediated transformation method (He et al., 2017), and were held overnight in the dark at 22°C before confocal imaging using a Leica-SP8.

Quantification of Fe content

Seedlings under indicated treatments were washed in Milli-Q H_2O twice, immersed for 5 min with 1 mM Na_2-EDTA solution twice, and then rinsed twice again with Milli-Q H_2O. Sampled tissues were dried in an oven at 80°C for 2 days and digested in 1 ml 65% HNO_3 for at least 2 days at room temperature. Then the samples were boiled for 1–2 h until completely digested and diluted with 12 ml Milli-Q H_2O. Fe contents were determined using inductively coupled plasma mass spectrometry (ICP-MS) as described (Meng et al., 2016).

Perls/DAB staining

Fe accumulation pattern in *Arabidopsis* roots was visualized using Perls/DAB staining as previously described (Roschzttardtz et al., 2013), with minor modification. Briefly, seedlings grown on ½ MS medium were treated with or without Fe starvation for 3 days. Perls/DAB staining was performed by vacuum infiltrating plant samples with Perls stain solution (4% HCl [v/v] and 4% [w/v] potassium ferrocyanide) for 30 min, and incubating for another 1.5 h. The reaction was stopped by rinsing the samples three times with distilled water, and the samples were further incubated in a methanol solution containing 0.01 M NaN_3 and 0.3% (v/v) H_2O_2 for 1 h before being washed with 0.1 M phosphate buffer (pH 7.4). For the intensification reaction, samples were incubated for 5 min in 0.1 M phosphate buffer (pH 7.4) solution containing 0.025% (w/v) DAB (Sigma) and 0.005% (v/v) H_2O_2. The reaction was stopped by rinsing with distilled water several times, and the samples were cleared in HCG solution (1 g/ml chloral hydrate in 15% glycerol) as described (Dong et al., 2017). Perls/DAB stain was imaged using a Nikon-ECLIPSE 80i.

Analysis of xylem sap

Xylem sap was collected as previously described (Sunarpi et al., 2005). Briefly, plants were grown in soil until bolting stage. After removal of the rosette leaves, the inflorescence stem was cut with a sharp razor blade. Xylem sap exudation was facilitated by covering the plants with a plastic dome. The first droplets were abandoned to avoid contamination and then the xylem sap was collected with a micropipette. Fifty-microliter xylem sap samples were diluted with 3 ml of 2% HNO_3 for subsequent measurement of Fe content by ICP-MS.

SUPPLEMENTAL INFORMATION

Supplemental information is available at *Plant Communications Online*.

FUNDING

This research was supported by the Strategic Priority Research Program of the Chinese Academy of Sciences (XDB27020101), the National Key

R&D Program of China (2016YFD0100700), and in part by the Ministry of Agriculture of China for Transgenic Research (2016ZX08009003-005-003).

AUTHOR CONTRIBUTIONS

S.C. and J.G. designed the research. S.C. performed most of the experiments. T.G., Z.Q., J.Y., Z.F., and Y.L. performed part of the experiments on Fe content determination and electrophysiological analysis. Z.F. and S.C. did the ^{15}N uptake assay. S.C. and H.L investigated the protein subcellular localization *in planta*. S.C., H.L., and J.G. wrote the manuscript.

ACKNOWLEDGMENTS

We thank Dr. Fang Xie (Center for Excellence in Molecular Plant Sciences, CAS) for kindly providing markers for the subcellular localization assay. No conflict of interest declared.

Received: June 4, 2021
Revised: August 26, 2021
Accepted: September 16, 2021
Published: September 20, 2021

REFERENCES

Alejandro, S., Cailliatte, R., Alcon, C., et al. (2017). Intracellular Distribution of Manganese by the Trans-Golgi Network Transporter NRAMP2 Is Critical for Photosynthesis and Cellular Redox Homeostasis. Plant Cell **29**:3068–3084.

Araki, R., Kousaka, K., Namba, K., Murata, Y., and Murata, J. (2015). 2'-Deoxymugineic acid promotes growth of rice (Oryza sativa L.) by orchestrating iron and nitrate uptake processes under high pH conditions. Plant J. **81**:233–246.

Chen, H., Zhang, Q., Cai, H., Zhou, W., and Xu, F. (2018). H2 O2 mediates nitrate-induced iron chlorosis by regulating iron homeostasis in rice. Plant Cell Environ. **41**:767–781.

Chu, H.H., Chiecko, J., Punshon, T., Lanzirotti, A., Lahner, B., Salt, D.E., and Walker, E.L. (2010). Successful reproduction requires the function of Arabidopsis Yellow Stripe-Like1 and Yellow Stripe-Like3 metal-nicotianamine transporters in both vegetative and reproductive structures. Plant Physiol. **154**:197–210.

Clough, S.J., and Bent, A.F. (1998). Floral dip: a simplified method for Agrobacterium-mediated transformation of Arabidopsis thaliana. Plant J. **16**:735–743.

Connolly, E.L., Campbell, N.H., Grotz, N., Prichard, C.L., and Guerinot, M.L. (2003). Overexpression of the FRO2 ferric chelate reductase confers tolerance to growth on low iron and uncovers posttranscriptional control. Plant Physiol. **133**:1102–1110.

Connorton, J.M., Balk, J., and Rodriguez-Celma, J. (2017). Iron homeostasis in plants - a brief overview. Metallomics **9**:813–823.

Conte, S.S., Chu, H.H., Rodriguez, D.C., Punshon, T., Vasques, K.A., Salt, D.E., and Walker, E.L. (2013). Arabidopsis thaliana Yellow Stripe1-Like4 and Yellow Stripe1-Like6 localize to internal cellular membranes and are involved in metal ion homeostasis. Front. Plant Sci. **4**:283.

Corratge-Faillie, C., and Lacombe, B. (2017). Substrate (un)specificity of Arabidopsis NRT1/PTR FAMILY (NPF) proteins. J. Exp. Bot. **68**:3107–3113.

Curie, C., Cassin, G., Couch, D., Divol, F., Higuchi, K., Le Jean, M., Misson, J., Schikora, A., Czernic, P., and Mari, S. (2009). Metal movement within the plant: contribution of nicotianamine and yellow stripe 1-like transporters. Ann. Bot. **103**:1–11.

DiDonato, R.J., Jr., Roberts, L.A., Sanderson, T., Eisley, R.B., and Walker, E.L. (2004). Arabidopsis Yellow Stripe-Like2 (YSL2): a metal-regulated gene encoding a plasma membrane transporter of nicotianamine-metal complexes. Plant J. **39**:403–414.

Divol, F., Couch, D., Conejero, G., Roschzttardtz, H., Mari, S., and Curie, C. (2013). The arabidopsis YELLOW STRIPE LIKE4 and 6 transporters control iron release from the chloroplast. Plant Cell **25**:1040–1055.

Dong, J., Pineros, M.A., Li, X., Yang, H., Liu, Y., Murphy, A.S., Kochian, L.V., and Liu, D. (2017). An arabidopsis ABC transporter mediates phosphate deficiency-induced remodeling of root architecture by modulating iron homeostasis in roots. Mol. Plant **10**:244–259.

Gong, J.M., Waner, D.A., Horie, T., Li, S.L., Horie, R., Abid, K.B., and Schroeder, J.I. (2004). Microarray-based rapid cloning of an ion accumulation deletion mutant in Arabidopsis thaliana. Proc. Natl. Acad. Sci. U S A **101**:15404–15409.

Green, L.S., and Rogers, E.E. (2004). FRD3 controls iron localization in Arabidopsis. Plant Physiol. **136**:2523–2531.

Haydon, M.J., and Cobbett, C.S. (2007). A novel major facilitator superfamily protein at the tonoplast influences zinc tolerance and accumulation in Arabidopsis. Plant Physiol. **143**:1705–1719.

Haydon, M.J., Kawachi, M., Wirtz, M., Hillmer, S., Hell, R., and Kramer, U. (2012). Vacuolar nicotianamine has critical and distinct roles under iron deficiency and for zinc sequestration in arabidopsis. Plant Cell **24**:724–737.

He, Y.N., Peng, J.S., Cai, Y., Liu, D.F., Guan, Y., Yi, H.Y., and Gong, J.M. (2017). Tonoplast-localized nitrate uptake transporters involved in vacuolar nitrate efflux and reallocation in Arabidopsis. Sci. Rep. **7**:6417.

Hindt, M.N., Akmakjian, G.Z., Pivarski, K.L., Punshon, T., Baxter, I., Salt, D.E., and Guerinot, M.L. (2017). BRUTUS and its paralogs, BTS LIKE1 and BTS LIKE2, encode important negative regulators of the iron deficiency response in Arabidopsis thaliana. Metallomics **9**:876–890.

Inoue, H., Kobayashi, T., Nozoye, T., Takahashi, M., Kakei, Y., Suzuki, K., Nakazono, M., Nakanishi, H., Mori, S., and Nishizawa, N.K. (2009). Rice OsYSL15 is an iron-regulated iron(III)-Deoxymugineic acid transporter expressed in the roots and is essential for iron uptake in early growth of the seedlings. J. Biol. Chem. **284**:3470–3479.

Klatte, M., Schuler, M., Wirtz, M., Fink-Straube, C., Hell, R., and Bauer, P. (2009). The analysis of Arabidopsis nicotianamine synthase mutants reveals functions for nicotianamine in seed iron loading and iron deficiency responses. Plant Physiol. **150**:257–271.

Krouk, G., Lacombe, B., Bielach, A., Perrine-Walker, F., Malinska, K., Mounier, E., Hoyerova, K., Tillard, P., Leon, S., Ljung, K., et al. (2010). Nitrate-regulated auxin transport by NRT1.1 defines a mechanism for nutrient sensing in plants. Dev. Cell **18**:927–937.

Leran, S., Varala, K., Boyer, J.C., Chiurazzi, M., Crawford, N., Daniel-Vedele, F., David, L., Dickstein, R., Fernandez, E., Forde, B., et al. (2014). A unified nomenclature of NITRATE TRANSPORTER 1/ PEPTIDE TRANSPORTER family members in plants. Trends Plant Sci. **19**:5–9.

Lin, S.H., Kuo, H.F., Canivenc, G., Lin, C.S., Lepetit, M., Hsu, P.K., Tillard, P., Lin, H.L., Wang, Y.Y., Tsai, C.B., et al. (2008). Mutation of the Arabidopsis NRT1.5 nitrate transporter causes defective root-to-shoot nitrate transport. Plant Cell **20**:2514–2528.

Liu, K.H., Huang, C.Y., and Tsay, Y.F. (1999). CHL1 is a dual-affinity nitrate transporter of arabidopsis involved in multiple phases of nitrate uptake. Plant Cell **11**:865–874.

Liu, X., Cui, H., Li, A., Zhang, M., and Teng, Y. (2015). The nitrate transporter NRT1.1 is involved in iron deficiency responses in Arabidopsis. J. Plant Nutr. Soil Sci. **178**:601–608.

Long, T.A., Tsukagoshi, H., Busch, W., Lahner, B., Salt, D.E., and Benfey, P.N. (2010). The bHLH transcription factor POPEYE regulates response to iron deficiency in arabidopsis roots. Plant Cell **22**:2219–2236.

Luo, J.S., Huang, J., Zeng, D.L., Peng, J.S., Zhang, G.B., Ma, H.L., Guan, Y., Yi, H.Y., Fu, Y.L., Han, B., et al. (2018). A defensin-like protein drives cadmium efflux and allocation in rice. Nat. Commun. **9**:645.

Mao, Q.Q., Guan, M.Y., Lu, K.X., Du, S.T., Fan, S.K., Ye, Y.-Q., Lin, X.Y., and Jin, C.W. (2014). Inhibition of nitrate transporter 1.1-controlled nitrate uptake reduces cadmium uptake in arabidopsis. Plant Physiol. **166**:934–U730.

Mendoza-Cozatl, D.G., Xie, Q., Akmakjian, G.Z., Jobe, T.O., Patel, A., Stacey, M.G., Song, L., Demoin, D.W., Jurisson, S.S., Stacey, G., et al. (2014). OPT3 is a component of the iron-signaling network between leaves and roots and misregulation of OPT3 leads to an over-accumulation of cadmium in seeds. Mol. Plant **7**:1455–1469.

Meng, S., Peng, J.S., He, Y.N., Zhang, G.B., Yi, H.Y., Fu, Y.L., and Gong, J.M. (2016). Arabidopsis NRT1.5 mediates the suppression of nitrate starvation-induced leaf senescence by modulating foliar potassium level. Mol. Plant **9**:461–470.

Munos, S., Cazettes, C., Fizames, C., Gaymard, F., Tillard, P., Lepetit, M., Lejay, L., and Gojon, A. (2004). Transcript profiling in the chl1-5 mutant of Arabidopsis reveals a role of the nitrate transporter NRT1.1 in the regulation of another nitrate transporter, NRT2.1. Plant Cell **16**:2433–2447.

Nikolic, M., and Romheld, V. (2003). Nitrate does not result in iron inactivation in the apoplast of sunflower leaves. Plant Physiol. **132**:1303–1314.

Nikolic, M., Cesco, S., Römheld, V., Varanini, Z., and Pinton, R. (2007). Short-term interactions between nitrate and iron nutrition in cucumber. Funct. Plant Biol. **34**:402–408.

Nozoye, T., Nagasaka, S., Kobayashi, T., Takahashi, M., Sato, Y., Sato, Y., Uozumi, N., Nakanishi, H., and Nishizawa, N.K. (2011). Phytosiderophore efflux transporters are crucial for iron acquisition in graminaceous plants. J. Biol. Chem. **286**:5446–5454.

Ravet, K., Touraine, B., Kim, S.A., Cellier, F., Thomine, S., Guerinot, M.L., Briat, J.-F., and Gaymard, F. (2009). Post-translational regulation of AtFER2 ferritin in response to intracellular iron trafficking during fruit development in arabidopsis. Mol. Plant **2**:1095–1106.

Riaz, N., and Guerinot, M.L. (2021). All together now: regulation of the iron deficiency response. J. Exp. Bot. **72**:2045–2055.

Roschzttardtz, H., Seguela-Arnaud, M., Briat, J.F., Vert, G., and Curie, C. (2011). The FRD3 citrate effluxer promotes iron nutrition between symplastically disconnected tissues throughout Arabidopsis development. Plant Cell **23**:2725–2737.

Roschzttardtz, H., Conejero, G., Divol, F., Alcon, C., Verdeil, J.L., Curie, C., and Mari, S. (2013). New insights into Fe localization in plant tissues. Front. Plant Sci. **4**:350.

Santi, S., and Schmidt, W. (2009). Dissecting iron deficiency-induced proton extrusion in Arabidopsis roots. New Phytol. **183**:1072–1084.

Siso-Terraza, P., Luis-Villarroya, A., Fourcroy, P., Briat, J.F., Abadia, A., Gaymard, F., Abadia, J., and Alvarez-Fernandez, A. (2016). Accumulation and secretion of coumarinolignans and other coumarins in Arabidopsis thaliana roots in response to iron deficiency at high pH. Front. Plant Sci. **7**:1711.

Smarrelli, J., and Castignetti, D. (1988). Iron assimilation in plants - reduction of a ferriphytosiderophore by nadh-nitrate reductase from squash. Planta **173**:563–566.

Smolders, A.J.P., Hendriks, R.J.J., Campschreur, H.M., and Roelofs, J.G.M. (1997). Nitrate induced iron deficiency chlorosis in Juncus acutiflorus. Plant Soil **196**:37–45.

SunarpiHorie, T., Motoda, J., Kubo, M., et al. (2005). Enhanced salt tolerance mediated by AtHKT1 transporter-induced Na unloading from xylem vessels to xylem parenchyma cells. Plant J **44**:928–938.

Tissot, N., Robe, K., Gao, F., Grant-Grant, S., Boucherez, J., Bellegarde, F., Maghiaoui, A., Marcelin, R., Izquierdo, E., Benhamed, M., et al. (2019). Transcriptional integration of the responses to iron availability in Arabidopsis by the bHLH factor ILR3. New Phytol. **223**:1433–1446.

Tsay, Y.F., Schroeder, J.I., Feldmann, K.A., and Crawford, N.M. (1993). The herbicide sensitivity gene CHL1 of Arabidopsis encodes a nitrate-inducible nitrate transporter. Cell **72**:705–713.

Vert, G., Grotz, N., Dedaldechamp, F., Gaymard, F., Guerinot, M.L., Briat, J.F., and Curie, C. (2002). IRT1, an Arabidopsis transporter essential for iron uptake from the soil and for plant growth. Plant Cell **14**:1223–1233.

Watanabe, S., Takahashi, N., Kanno, Y., Suzuki, H., Aoi, Y., Takeda-Kamiya, N., Toyooka, K., Kasahara, H., Hayashi, K.I., Umeda, M., et al. (2020). The Arabidopsis NRT1/PTR FAMILY protein NPF7.3/NRT1.5 is an indole-3-butyric acid transporter involved in root gravitropism. Proc. Natl. Acad. Sci. U S A **117**:31500–31509.

Waters, B.M., Chu, H.H., Didonato, R.J., Roberts, L.A., Eisley, R.B., Lahner, B., Salt, D.E., and Walker, E.L. (2006). Mutations in Arabidopsis yellow stripe-like1 and yellow stripe-like3 reveal their roles in metal ion homeostasis and loading of metal ions in seeds. Plant Physiol. **141**:1446–1458.

Zhai, L., Xiao, D., Sun, C., Wu, T., Han, Z., Zhang, X., Xu, X., and Wang, Y. (2016). Nitric oxide signaling is involved in the response to iron deficiency in the woody plant Malus xiaojinensis. Plant Physiol. Biochem. **109**:515–524.

Zhai, Z., Gayomba, S.R., Jung, H.I., Vimalakumari, N.K., Pineros, M., Craft, E., Rutzke, M.A., Danku, J., Lahner, B., Punshon, T., et al. (2014). OPT3 is a phloem-specific iron transporter that is essential for systemic iron signaling and redistribution of iron and cadmium in arabidopsis. Plant Cell **26**:2249–2264.

Zhang, L., Hu, B., Deng, K., Gao, X., Sun, G., Zhang, Z., Li, P., Wang, W., Li, H., Zhang, Z., et al. (2019). NRT1.1B improves selenium concentrations in rice grains by facilitating selenomethinone translocation. Plant Biotechnol. J. **17**:1058–1068.

Zhao, T., and Ling, H.Q. (2007). Effects of pH and nitrogen forms on expression profiles of genes involved in iron homeostasis in tomato. Plant Cell Environ. **30**:518–527.